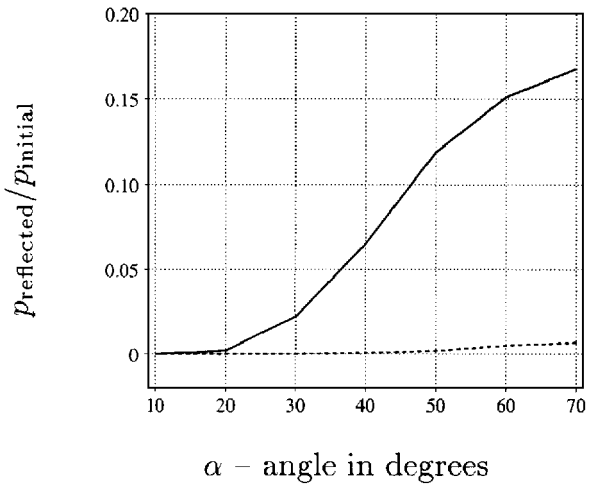

Fig. 3 Normalized pressure perturbation evolution as the vortex passes out of the domain vs angle of incidence on boundary measured from normal: - - - -, proposed zonal boundary condition; and ——, Thompson boundary condition.

an angle to the boundary as the initial condition. The waves propagate toward the inflow boundary. The boundary zone is 2.5λ wide where λ is the acoustic wavelength. Other boundary parameters are $U_{o_l} = 1.15c_\infty$, $\sigma_{o_l} = 0.035c_\infty/\lambda$, and f_l in Eq. (5) is set so that $U(X_{\max} - W_{U_l}) = 0.01c_\infty$. The transverse boundaries are periodic. Reflection amplitudes are plotted in Fig. 3 as a function of angle. The reflected amplitude would be zero for an ideal boundary condition. The zonal boundary condition is seen to perform significantly better than the Thompson boundary condition, especially at angles away from normal incidence.

Reflections are strongly dependent on zone size, and accuracy may be increased by increasing the size of the zones.

Conclusions

A simple new zonal boundary condition has been proposed. It is based upon the addition of dissipative and convective terms to the compressible Navier–Stokes equations. The scheme has been analyzed using a one-dimensional model equation and validated with two model problems. Boundary reflections are very significantly reduced compared to the local boundary condition of Thompson.

Acknowledgment

We are very grateful to Ted Manning, who performed the vortex computations.

References

[1]Enquist, B., and Majda, A., "Absorbing Boundary Conditions for the Numerical Simulation of Waves," *Mathematics of Computation*, Vol. 31, No. 139, 1977, pp. 629–651.

[2]Gustafsson, B., "Far-Field Boundary Conditions for Time-Dependent Hyperbolic Systems," *SIAM Journal of Scientific and Statistical Computing*, Vol. 9, No. 5, 1988, pp. 812–828.

[3]Giles, M. B., "Nonreflecting Boundary Conditions for Euler Equations Calculations," *AIAA Journal* Vol. 18, No. 12, 1990, 2050–2058.

[4]Tam, C. K. W., and Dong, Z., "Radiation and Outflow Boundary Conditions for Direct Computation of Acoustic and Flow Disturbances in a Nonuniform Mean Flow," AIAA Paper 95-007, June 1995.

[5]Hayder, M. E., and Turkel, E., "Nonreflecting Boundary Conditions for Jet Flow Computations," *AIAA Journal*, Vol. 33, No. 12, 1995, pp. 2264–2270.

[6]Givoli, D., *Numerical Methods for Problems in Infinite Domains*, Elsevier, Amsterdam, 1992.

[7]Grote, M., "Nonreflecting Boundary Conditions," Ph.D. Thesis, Mathematics Dept., Stanford Univ., Stanford, CA, 1995.

[8]Colonius, T., Lele, S. K., and Moin, P., "Boundary Conditions for Direct Computation of Aerodynamic Sound Generation," *AIAA Journal*, Vol. 31, No. 9, 1993, pp. 1574–1582.

[9]Rai, M. M., and Moin, P., "Direct Numerical Simulation of Transition and Turbulence in a Spatially Evolving Boundary Layer," *Journal of Computational Physics*, Vol. 109, No. 2, 1993, pp. 169–192.

[10]Ta'asan, S., and Nark, D. M., "An Absorbing Buffer Zone Technique for Acoustic Wave Propagation," AIAA Paper 95-0146, Jan. 1995.

[11]Berenger, J. P., "A Perfectly Matched Layer for the Absorption of Electromagnetic Waves," *Journal of Computational Physics*, Vol. 114, No. 2, 1994, pp. 185–200.

[12]Hu, F. Q., "On Absorbing Boundary Conditions for Linearized Euler Equations by a Perfectly Matched Layer," Inst. for Computer Applications in Science and Engineering, Rept. 95-70, Hampton, VA, 1995.

[13]Thompson, K. W., "Time-Dependent Boundary Conditions for Hyperbolic Systems," *Journal of Computational Physics*, Vol. 68, No. 1, 1987, pp. 1–24.

[14]Colonius, T., Lele, S. K., and Moin, P., "The Free Compressible Viscous Vortex," *Journal of Fluid Mechanics*, Vol. 230, Sept. 1991, pp. 45–73.

S. Glegg
Associate Editor

Diffusion Flame Adjacent to a Rotating Solid Fuel Disk in Zero Gravity

Joe M. Holcomb*
NYMA Inc., Brook Park, Ohio 44135
and
James S. T'ien†
Case Western Reserve University, Cleveland, Ohio 44106-7222

Introduction

In the past, a number of studies have examined the characteristics of one-dimensional laminar stagnation-point diffusion flames burning adjacent to solid fuel surfaces. The stagnation flowfield in these past studies has been created by free or forced convection, i.e., by buoyancy effects or by an air jet impinging on the fuel surface (see, for example, Refs. 1 and 2). The focus of the current study is to examine the characteristics of a diffusion flame established adjacent to an infinitely large rotating solid-fuel disk in the absence of buoyancy forces. In this different type of one-dimensional diffusion flame, the flowfield is created by rotation of the fuel disk and the viscosity of the gases next to the disk. For laminar, incompressible, nonreacting flow, this problem is reduced to the well-known von Kármán rotating disk problem.[3] A similarity solution is possible, which is an exact solution of the Navier–Stokes equations. Heat transfer in a compressible flow adjacent to a rotating disk has been treated by Ostrach and Thornton.[4] The first work involving combustion of a rotating disk is by Vedha-Nayagam et al.,[5] in which a diffusion flame analysis has been performed under the assumption of infinitely fast kinetics. In the present work, we extend the analysis to include a finite-rate chemical reaction and surface thermal radiation loss. This enables us to study the question of flame extinction and the flame behavior at low disk rotation rates. The flammability of a rotating subject can be an important consideration in spacecraft fire safety.

Theoretical Model

The combustion model used here assumes the following: a one-step forward gas-phase reaction of second order occurs near the fuel surface, all gases and mixtures of gases follow the ideal gas law, the product of density and viscosity is constant, the diffusion coefficients of all gas species are equal, the specific heats of the gas species are constant and equal, the Prandtl (Pr) and Schmidt (Sc) numbers

Received July 30, 1996; revision received Dec. 6, 1996; accepted for publication Dec. 20, 1996.

*Research Engineer.
†Professor, Department of Mechanical and Aerospace Engineering. Associate Fellow AIAA.

are constant, the pyrolysis of the solid fuel follows an Arrhenius law, the temperature profile in the solid is one-dimensional and exponential (i.e., the solid disk thickness is much larger than the solid thermal-diffusional length), and gas-phase radiation is negligible. These assumptions and the property values are the same as those used in Refs. 1 and 2 so that proper comparison can be made to assess the effects of different flow types on the flame.

The fluid dynamics model used here is basically the same as that in Ref. 4. It is an axisymmetric flow problem with three velocity components. Zero gravity is assumed. The governing nondimensional equations in cylindrical coordinates are the following:

$$f = \tfrac{1}{2}h', \qquad h''' + hh'' = \tfrac{1}{2}(h'^2 - 4g^2)$$

$$g'' + hg' - h'g = 0, \qquad (1/Pr)\theta'' - h\theta' = q\omega$$

$$(1/Sc)Y_f'' - hY_f' = \omega, \qquad (1/Sc)Y_o'' - hY_o' = N_o\omega$$

with $f(\eta) = v_r/(\Omega r)$, $g(\eta) = v_\phi/(\Omega r)$, $h(\eta) = (\rho/\rho_\infty)v_z/(\Omega\nu_\infty)^{1/2}$, and $\theta = T/T_\infty$ where v_r, v_ϕ, and v_z are the velocity components in the radial (r), tangential (ϕ), and axial (z) directions, respectively; Ω is the rotation rate of the solid fuel in rad/s; Y_f and Y_o are the mass fraction of fuel vapor and oxygen; and ν_∞, ρ_∞, and T_∞ are the kinematic viscosity, density, and temperature in the freestream, respectively. The derivative ($'$) is $\mathrm{d}/\mathrm{d}\eta$, where η is the nondimensional axial distance given by the Howarth transformation

$$\eta = (\Omega/\nu_\infty)^{\frac{1}{2}} \int \left(\frac{\rho}{\rho_\infty}\right) \mathrm{d}z$$

The nondimensional reaction rate is given by $\omega = DY_fY_o \exp(-E/\theta)$, $D = B/\Omega$, B is the modified frequency factor in the gas-phase reaction, and E is the dimensionless activation energy.

The boundary conditions at the surface ($\eta = 0$) are

$$h_w' = 0, \quad g_w = 1, \quad Y_{fw}' = Sch_w(1 - Y_{fw}), \quad Y_{ow}' = Sch_wY_{ow}$$

$$\theta_w' = -Prh_w[\theta_w + L - (c_s/c_p)] + S\theta_w^4$$

$$h_w = -A\exp(-E_w/\theta_w)$$

where $A = b/(\rho_\infty\mu_\infty\Omega)^{1/2}$, b is the preexponential factor in surface pyrolysis relation, L is the dimensionless latent heat, $S = (\sigma\epsilon T_\infty^3/\lambda_\infty)(\mu_\infty/\rho_\infty\Omega)^{1/2}$, and ϵ is the emissivity of the solid. The effect of background radiation on the burning process was investigated and found to be small. Therefore, it was neglected for the current computations to facilitate comparisons with previous flame computations for forced and buoyant flow cases. Note that S, the surface radiative loss parameter, is proportional to $\Omega^{-1/2}$. At small rotation rate, S is amplified and the rotation rate Ω plays a similar role as the stretch rate in the stagnation flame problem.

The remaining five boundary conditions are applied at freestream ($\eta \to \infty$). These are

$$h_\infty' = 0, \qquad g_\infty = 0, \qquad Y_{f\infty} = 0$$

$$Y_{o\infty} = \text{user specified constant}, \qquad \theta_\infty = 1$$

Certain physical quantities must be chosen to solve this set of equations. These include things such as the ambient temperature, the atmospheric composition, and the fuel to be burned. The atmosphere is chosen to be a nitrogen and oxygen mixture at a temperature of 300 K. The fuel is chosen to be polymethylmethacrylate for consistency with previous studies. The properties of the fuel and atmosphere are the same as those used in Refs. 1 and 2.

The governing set of equations is solved by using an explicit finite-difference numerical scheme. A time-marching term is introduced into the differential equations. Appropriate initial conditions are chosen, and the scheme marches in time to a converged steady-state flame solution or to an extinction solution. As with previous work,[1,2] grid and domain independence have been checked. This solution provides the three velocity components, the fuel and oxidizer concentration levels, and the temperature distribution for the case under investigation.

Results and Discussion

The computed temperature and species profiles are found to be qualitatively similar to those in the stagnation flame cases. The computed velocity profiles are also similar to that in Refs. 4 and 5. Consequently, detailed flame structure will not be shown here. We will concentrate our discussion on the global results from a parametric study varying the rotation rate, the ambient oxygen mass fraction, and the solid emissivity.

For $Y_\infty = 0.2324$ (air), the peak flame temperatures as a function of rotation rate are shown in Fig. 1 for both the case with surface radiative loss ($\epsilon = 1$) and the case without surface radiative loss ($\epsilon = 0$). Also presented for comparison are the flame temperatures of the stagnation flame in forced flow ($\epsilon = 1$ only) as a function of the stretch rate a_f. Note that to be able to present the results compactly in one figure, the rotation rate coordinate used is $\Omega/12$ instead of Ω. Figure 2 shows that without radiative loss (but with finite-rate kinetics), there exists a high rotation-rate blowoff limit as indicated by the slope of θ_f approaching vertical. But the flame temperature

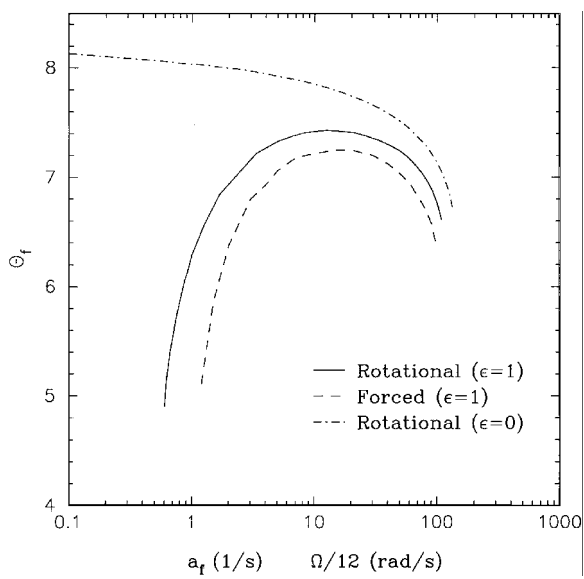

Fig. 1 Peak flame temperature as a function of rotation rate Ω for cases both with ($\epsilon = 1$) and without ($\epsilon = 0$) surface radiative loss. Also shown for comparison is the peak flame temperature for the purely forced-flow stagnation diffusion flame ($\epsilon = 1$) as a function of stretch rate a_f. The oxygen mass fraction $Y_{o_\infty} = 0.2324$ (air).

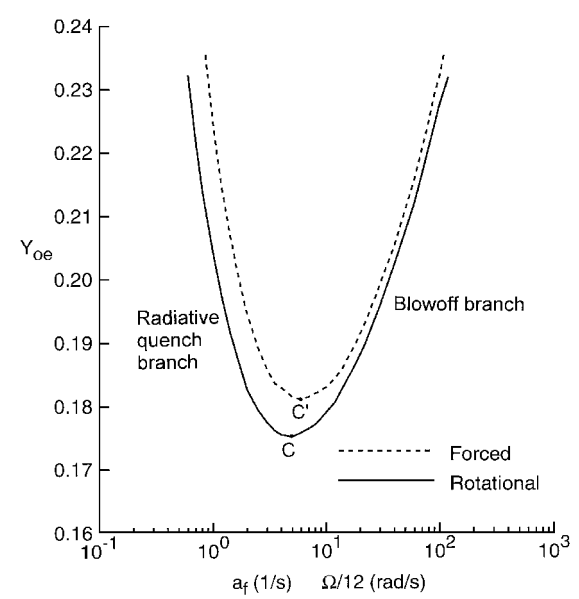

Fig. 2 Flammability boundaries for rotational and forced-stagnation-flow cases.

increases with decreasing rotation rate and there appears to be no extinction limit at low rotation rate. With radiative loss, flame temperature drops at low rotation rate as a result of amplification of the surface radiative loss parameter S and a radiative quench limit exists at sufficiently low rotation rate. The existence of the blowoff and quench limits with respect to rotation rate for this problem is similar to those found previously in forced-flow stagnation flames,[1] as shown in Fig. 1. However, the maximum flame temperature is higher for the rotational case (7.4 at $\Omega = 156$ rad/s) compared to 7.2 at $a_f = 15$ 1/s for the forced case. This has consequences for the low oxygen limit, which is discussed next.

Using oxygen mass fraction and rotation rate, flammability boundaries are shown in Fig. 2. For the rotational case, it consists of a blowoff branch at high rotation rates and a radiative quench branch at low rotation rates. The merging point (C) between the two branches defines the critical oxygen limit below which the solid disk will not be flammable at any rotational rate. The shape and the physical interpretation of this boundary is similar to the one derived in a previous study of forced-flow stagnation diffusion flame,[1] which is also plotted in Fig. 2 for comparison. Despite the similarity of shape between the two boundaries, the critical oxygen mass fraction for the rotational case (as indicated by point C) is lower than that for the forced flow case (as indicated by point $C1$). This is consistent with the finding in Fig. 1 that the maximum flame temperature for the rotational case is higher.

In Ref. 2, the flammability boundary for buoyancy-induced stagnation diffusion flame was compared to that for the forced-flow stagnation diffusion flame. The two boundaries can be collapsed into one if a properly defined buoyant stretch rate is adopted and the critical low oxygen limits are essentially the same for the two cases. Thus, the critical oxygen limit for the rotational solid is lower than that for the solid in buoyant flow as well.

An additional remark can be made on the influence of gas (flame) radiation. The recent addition of flame radiation to the model in Ref. 1 indicates a slight shift of the quenching boundary.[6] But for solid fuel with high surface temperature, the surface radiative loss dominates and this modification is very modest. We expect that the comparison between the rotational case and the forced and buoyant stagnation flame cases will remain true when flame radiation is included.

Concluding Remarks

Diffusion flame adjacent to a large, rotating solid fuel disk in the absence of buoyant force is modeled and numerically solved in this work. Similar to the conventional stagnation diffusion flame problems, the temperature and species distributions of this rotational flame are found to be one dimensional.[5] But unlike the stagnation-point problems, where the flow is two dimensional, driven either by inertia (forced convection) or by buoyancy, the flow in this problem is three dimensional, driven by a rotating solid through gas viscosity.

With the inclusion of a one-step finite-rate gas-phase reaction and a surface radiative loss term, the model predicts the existence of a blowoff extinction limit at high rotation rate because of insufficient gas residence time and a quenching limit at low rotation rate because of excessive radiative loss. The existence of these limits and the general flame behavior are similar to those in stagnation-point diffusion flames studied previously, with rotation rate playing the role of stretch rate. However, the different flowfield produces an important quantitative difference: the critical low oxygen percentage that can sustain a solid-fuel diffusion flame in the rotational case is lower than those in the stagnation flame cases. This suggests that a slow-rotating solid in a quiescent ambient can be more flammable than a stationary solid in a flowing stream, a result that should have implications for fire safety consideration in spacecraft. An ongoing research project may provide the needed experimental data for this prediction.

Acknowledgments

J.S.T. would like to acknowledge support for this work by the Microgravity Science and Applications Division of NASA Headquarters through Grant NAG3-1046. We thank M. Vedha-Nayagam for communicating unpublished results.

References

[1]T'ien, J. S., "Diffusion Flame Extinction at Small Stretch Rates: The Mechanism of Radiative Loss," *Combustion and Flame*, Vol. 65, No. 1, 1986, pp. 31–34.

[2]Foutch, D. W., and T'ien, J. S., "Extinction of a Stagnation-Point Diffusion Flame at Reduced Gravity," *AIAA Journal*, Vol. 25, No. 7, 1987, pp. 972–976.

[3]Von Kármán, T., "Uber Laminare und Turbulent Reibunt," *Zeitschrift fur Angewandte Mathematik und Mechanik*, Bd. 1, Heft 4, Aug. 1921, pp. 233–252.

[4]Ostrach, S., and Thornton, P. R., "Compressible Laminar Flow and Heat Transfer About a Rotating Isothermal Disk," NACA TN 4320, 1958.

[5]Vedha-Nayagam, M., Midkiff, K. C., and Mahalingam, B., "Laminar Forced Convective Burning of a Rotating Disk in Microgravity," *Spring Technical Meeting, Central States Section*, The Combustion Inst., Pittsburgh, PA, 1990.

[6]Rhatigan, J. L., Bedir, H., and T'ien, J. S., "Gas-Phase Radiative Effects on the Burning and Extinction of a Solid Fuel," *Combustion and Flame* (submitted for publication).

K. Kailasanath
Associate Editor

Orthogonalization of Measured Modes—Revisited

Menahem Baruch*
Technion—Israel Institute of Technology, Haifa 32000, Israel

Introduction

THE orthogonalization of measured modes has been treated by Targoff,[1] Baruch and Bar-Itzhack,[2] and others. In Ref. 2 a closed-form solution has been found by minimization of the mass weighted distance between the orthogonalized and measured modes (see also Refs. 3 and 4). Recently, Zhang and Zerva[5] introduced a method in which they obtained the solution by minimization of the nonweighted distance between the orthogonalized and the measured modes. Here arises the interesting question: what is the right way to measure the distance between two matrices? The question of distance between two matrices is directly connected with the notion of length of a vector. The concept of length of a vector in static or dynamic surroundings is treated in Refs. 6 and 7.

Generalized Orthogonalization

Following Refs. 6 and 7 the generalized distance between two vectors $\boldsymbol{V}$ and $\boldsymbol{Z}$ can be defined as

$$\Delta\mathcal{E}^2 = (\boldsymbol{V} - \boldsymbol{Z})^t W(\boldsymbol{V} - \boldsymbol{Z}) = \left\| W^{\frac{1}{2}}(\boldsymbol{V} - \boldsymbol{Z}) \right\| \tag{1}$$

where $\|\cdot\|$ symbolizes the Euclidean norm and W is a positive definite matrix. Equation (1) can be generalized also for matrices.

Let $W_1(n \times n)$ and $W_2(n \times n)$ be two positive definite symmetric matrices. The generalized distance between the measured and the orthogonalized mode shapes will be in respect to W_1, and the mode shapes will be orthogonalized in respect to W_2 so that

$$X^t W_2 X = I \tag{2}$$

where $X(n \times m)$ are the orthogonalized mode shapes, n are the degrees of freedom of the structure, and m is the number of measured mode shapes.

Before the minimization process, every measured mode shape must be normalized:

$$T_i = \tilde{T}_i(\tilde{T}_i^t W_2 \tilde{T}_i)^{-\frac{1}{2}} \qquad i = 1 - m \tag{3}$$

Received Oct. 17, 1996; revision received Nov. 23, 1996; accepted for publication Nov. 27, 1996.

*Professor Emeritus, Faculty of Aerospace Engineering.